RSC Advances

ROYAL SOCIETY OF CHEMISTRY

www.rsc.org/advances

Hydrothermal-assisted biomimetic synthesis of brush-like Hap/PAN composite and its application for decontaminating the metal ions

Hehe Guo,[a, b] Huaijuan Zhou,[a, b] Ping Jin,[a,c] Wenjing Li,[a,b] Yining Ma, [a, b] Ioku Koji[d,] and Shi-dong Ji[a,*]

[a]State Key Laboratory of High Performance Ceramics and Superfine Microstructure, Shanghai Institute of Ceramics, Chinese Academy of Sciences, Shanghai 200050, China

[b]University of Chinese Academy of Sciences, Beijing 100049, China

[c]Materials Research Institute for Sustainable Development, National Institute of Advanced Industrial Science and Technology, Nagoya 463-8560, Japan

[d]Faculty of Economics, Keio University, Building #2-101B, 4-1-1, Hiyoshi, Kohoku-ku, Yokohama 223-8521, Japan

ABSTRACT: In this work, a novel biomimetic mat consisting of brush-like polyacrylonitrile (PAN) - hydroxyapatite (Hap) composite fibers was successfully prepared by means of a combination of two simple but effective methods - electrospinning technology and vapor hydrothermal treatment. The backbone of the fiber is the PAN fiber with the diameter of 2-3 μm and the lateral branch is the Hap nanowires. In the biomimetic process, calcium phosphate (TCP) worked as the seed and it

transferred to Hap nanowire in situ and pierced the PAN fiber when it was cultured under high temperature vapor. This mat is an ideal candidate material for decontaminating the metal ions in terms of its convenience of recycle and the high specific surface area. The as-obtained materials were characterized with X-Ray diffractometer (XRD), transmission electron microscopy (TEM) and scanning electron microscopy (SEM). Moreover, the adsorption experiments of the PAN/Hap composite fiber mat for Pb^{2+} were conducted. The results exhibited that the maximum adsorption quantity of the composite fiber mat for heavy metal Pb^{2+} was up to 433 mg/g, and the Pb^{2+} adsorption process occurs through a two-step mechanism: rapid surface complexation followed by partial dissolution of hydroxyapatite and precipitation of pyromorphite.

KEYWORDS: hydroxyapatite; biomimetic process; electrospinning; vapor hydrothermal; composite fiber; heavy metal; adsorption.

1. Introduction

Since removal of heavy ions from industrial waste water is a vital step in water purification, depuration methods have been investigated for many years. To date, chemical precipitation, ion exchange, filtration, adsorption and electrochemical treatment have been typical approaches for wiping out the toxic metal ions from industrial waste water[1, 2]. Among these approaches, however, the method of adsorption by virtue of cost-effective and handy operation is capturing considerable researchers' attention, and therefore great efforts have been taken to develop new adsorbents such as activated carbons, biomass, zeolites, hydroxyapatite, natural and synthetic polymers. Hydroxyapatite have been reported to have a high adsorption capacity for the heavy metal ions

such as Pb, Hg, Zn, Cu, Cd, Co and Sb in aqueous solutions[2-5]. To improve the capacity of the removal metal ions, a variety of Hap nanopowders with a large special surface area have been synthesized [6-10]. Rosanna Gonzalez-McQuire synthesized aqueous colloids of amino rod-like acid-functionalized hydroxyapatitethe with the size of less than 80 nm in length and ca. 5 nm in width through the hydrothermal treatment[6]. As for work made by Minhua Cao's group, ultrahigh-aspect-ratio hydroxyapatite nanofibers with an aspect ratio of above 1000 were prepared in reverse micelles under hydrothermal conditions, and the length of the prepared-nanofibers can be up to several hundreds of micrometers and the diameter was about 50-120 nm[11]. Besides, in the absence of any surfactants, organic solvent or organic template-directing reagents, Kaili Lin successfully synthesized hydroxyapatite Hap nanoparticles, nanowires and hollow nano-structured microspheres on a large scale via a facile hydrothermal treatment of similarly structured hard-precursors of $CaCO_3$ nanoparticles, xonotlite nanowires and hollow $CaCO_3$ microspheres in Na_3PO_4 solution, respectively[9]. When it comes to the practical industrial applications, the drawback with respect to the dimension limit of all these materials appears. Hap nanopowders have difficulty in reclamation and the nano-size powders increase the tendency of particle agglomeration. Beyond that, if these nano-Hap powders are directly poured into waste water without further treatment, it'll bring about the second environmental pollution.

One effective method to solve these problems is to find suitable materials to fix the Hap. Preparing the fiber mats by means of the electrospinning is an effective way to hold the Hap - Zhang[12] reports a novel composite nanofibers of hydroxyapatite/chitosan prepared by combining an in situ co-precipitation synthesis approach with an electrospinning process. The obtained non-

woven mats play a major role in immobilizing the Hap powders. In addition to that, electrospun fibrous mats are advantageous because of their light weight, high aspect ratio and easy production. Moreover, the mats synthesized by electrospinning are usually porous, and therefore not only results in a high surface area arising from the open three-dimensional network, but may also permits the permeation of water, which is favorable in the process of water purification. Unfortunately, such structural materials also produce a serious problem that most Hap particles are coated by the polymer substance, which greatly cut down the effective specific surface area of Hap. To overcome this shortcoming, some researchers have tried a few methods to remove the polymer with the intention of obtaining Hap fiber mats. In order to remove the PVP polymer binder, oxygen plasma treatment has been adopted by Wang[13]. Actually, clearing away the polymer rather than the binder by means of high-temperature calcination with the purpose of burning off the polymer is the most common method. For example, Pierre-Alexis Mouthuy[14] burned the Poly (lactic-co-glycolic acid) up at 1100 ^{o}C, leaving the Hap fiber mats remained. Nevertheless, the connection force between the Hap particles decreases rapidly in the absence of polymer bonding effect and the nano-size Hap grains may be aggregate into larger ones during the process of high-temperature calcination, resulting in the decrease of specific surface area of Hap fiber mats.

In this work, Hap/PAN composite possessing a novel biomimetic microstructure was prepared by hydrothermal-assisted biomimetic process. This idea was inspired by the seed germination and growth afterward under proper conditions for turf. In our work, TCP worked as the plant seed and it would transfer to Hap in situ and pierce the fiber when it was cultured under high temperature vapor [15-17] . In the biomimetic process, tri-calcium phosphate (TCP) was first dispersed into the PAN

solution to obtain the suspension, and TCP/PAN fiber mats with TCP embedded into the PAN fibers were prepared by the electrospinning, then the obtained mats were treated by high temperature vapor. The non-woven mats were consisted of brush-like Hap/PAN composite fibers, where the in-situ grown Hap nanowires retain very high specific surface area and stick to the PAN subtract firmly. This mat material is an ideal candidate for decontaminating the metal ions in terms of its convenience of recycle and the high specific surface area.

2. Experience section

2.1 Materials：

All chemicals were analytical grade and were used as received without further purification. The reagents used in this study included calcium carbonate ($CaCO_3$, AR), ammonium dihydrogen phosphate ($NH_4H_2PO_4$, AR), N,N-dimethylformamide (DMF, AR) and polyacrylonitrile (PAN) with a molecular weight of 150000, lead nitrate ($Pb(NO_3)_2$, AR), which were purchased from the Aladdin reagent co.(Shanghai, China)

2.2 Preparation of PAN/TCP composite fiber mats:

In general, three processes were needed in sequence for the preparation of Hap/PAN composite fiber mats: Synthesis of beta-calcium phosphate (β-TCP), preparation of TCP/PAN composite mats, and growth of Hap nanowires on the PAN fiber.

1) Synthesis of β-TCP.

β-TCP – the precursor of Hap – was synthesized at the temperature of 1150 ^oC. $NH_4H_2PO_4$ and $CaCO_3$ were combined in a 2/3 molar ratio and milled in ethyl alcohol with an autonomous grinding machine for 4h. The slurry was dried in oven at 70 ^oC and the mixed powders were stored in a sealing bag before it was used. The mixed powders of $NH_4H_2PO_4$ and $CaCO_3$ were placed in a quartz

crucible and heated to 1150 °C in furnace with the heating rate of 8 °C/min and then maintained at 1150℃ for 5min. Afterwards, the sample was spontaneously cooled down in the furnace and then grinded for 4h. In the end, the synthesis sample was stored in sealing bag.

2) Preparation of PAN/TCP composite fiber mats.

For the common procedure, PAN was first dissolved in DMF at 35℃ to from a 15 wt% solution under vigorous stirring, then β-TCP powder was added into the PAN solution to form the electrospinning slurry and the slurry was stirred overnight until completely mixed (the mass ratio of β-TCP to PAN is 1:1). A freshly prepared electrospinning slurry ultrasoniced 20 minutes before used was loaded into a 20ml plastic syringe, and then the springer was equipped with a 0.8 mm in diameter stainless steel needle. In prior to electrospinning, all the bubbles from the slurry should be removed with special care. The flow rate was controlled at 0.8ml/h while the power of 16kV was supplied. The fiber mats were collected using stainless steel wire mesh collector placed 15cm away from the tip of the needle. During the Electrospinning, the ambient temperature was maintained at 25℃ and the humidity at 20 – 40 %. After the obtained PAN/TCP composite fiber mats were heated in an oven at 70℃ for 1h, they were ready for next-step experiment.

3) Growth of Hap nanowires on the PAN fiber.

The PAN/TCP composite fiber mats were set in a 105 cm^3 autoclave with 40 ml ion-exchanged water addition, then they were exposed to vapor of water under different temperature and time. After the as-prepared samples were dried at 60 °C, they were ready for characterization and performance evaluation.

2.3 Removal experiment of Pb^{2+} ion in aqueous water:

Adsorption experiments of Pb^{2+} ions by the PAN/Hap composite fiber mats (0.2 g) were conducted in 150 ml aqueous solution with controlled initial Pb^{2+} concentration and pH value. The different initial Pb^{2+} concentrations of the aqueous solution were prepared by dissolving the lead nitrate ($Pb(NO_3)_2$) in deionized water and the pH value of aqueous solution was adjusted to be 5.2 by adding 0.1 M NaOH and time-dependent the value of pH was measured by the pH meter.

The time-dependent Pb^{2+} concentrations in aqueous solution during removal experiences were measured by using an Inductively Coupled Plasma emission spectrometer (ICP). In order to calculate the adsorption capacity of PAN/Hap composite fiber mat, the following equation was used.

$$q_t = (C_0 - C_t)\mathrm{V}/\mathrm{m} \quad (1)$$

$$q_e = (C_0 - C_e)\mathrm{V}/\mathrm{m} \quad (2)$$

where q_e and q_t are the amount of metal ions adsorbed (mg/g) at equilibrium and at time t, respectively; C_0 and C_e are the concentrations (mg/l) of the initial lead ions and the final or equilibrium lead ions; V (L) is the volume of the solution; and m (g) is the weight of PAN/Hap composite fiber adsorbent in its dry state. All the experiments were performed in duplicate and the averaged values were recorded.

2.4 Materials characterization:

The phase of samples were characterized by the X-Ray diffraction (XRD) using a Rigaku Ultima IV diffractometer using CuKα radiation (λ = 1.5418Å) at 40 kV voltage and 40 mA current and identified by comparison with the date of the Joint Committee of Power Diffraction Standard (JCPDS) database, and the spectrum were collected in the 2ϑ range between 10 and 70 ° with 0.05 °

step and 5 °/min scan speed. Fourier transform infrared (FTIR) spectrum was recorded on a Thermo Nicolet iS10 Fourier spectrometer in the region of 400 - 4000 cm^{-1} with a resolution of 4 cm^{-1}. The morphologies and structures were studied by the scanning electron magnifications (SEM, HITACHI S-3400, Japan) at an acceleration voltage of 10 kV and the transmission electron microcopy (TEM, JEOL2010, Japan) operated at 200 kV, selected area electron diffraction (SAED). The composition of the fiber was also examined by energy dispersive X-ray spectrum (EDX) which was used to analyze the atomic ratio of Ca/P of the Hap.

3. Results and discussion

3.1 Characterization of TCP and TCP/PAN composite fiber mat:

PAN was chosen as the electrospun matrix because of its good spinnability, hydrophobicity and the higher melting point which is up to 300 ^{o}C.

The composition and phase purity of the products were first examined by XRD, and the results manifested that pure *β*-TCP was obtained under the high temperature of 1150 ^{o}C for 5 min. The corresponding XRD pattern of the product was shown in **Figure 1A**, and all the diffraction peaks can be ascribed to hexagonal TCP (JCPDS file, No. 09-0169, space group R-3c). Therefore, the synthesized product can be assigned to the pure phase of *β*-TCP. Fourier transform infrared (FTIR) spectroscopy can be seen in the Supporting Information (Figures S1). **Figure 1B** depicted SEM images of electrospun TCP/PAN fibers under low and high magnifications. It can be clearly observed that the TCP powders were embeded into the PAN fiber with the diameter of 2 - 3 μm.

3.2 Effect of vapor hydrothermal time and temperature on Hap/PAN composite fiber mat:

The phase of PAN/Hap composite fiber synthesised under saturated vapor at different temperatures and soaking period times were examined by XRD (**Figure 2A, 2C**). Compared with the PDF standard card of Hap (JCPDS file, No. 46-0905, space group P63/m, $Ca_9(HPO_4)(PO_4)_5OH$)), XRD of samples exhibited significantly higher intensity of the (002) diffraction peak. Along with the peaks associated with (211) (300) (112) and (202) (222) orientations, we could confirm the formation of the typical hexagonal structure of calcium deficiency hydroxyapatite (Hap) crystals. The higher intensity of the (002) diffraction peak indicted that the vapor hydrothermal grown Hap nanowires were preferentially oriented along the c-axis direction. And one peak at around 2θ=15° appeared, corresponding to the PAN polymer. The result confirmed that after vapor hydrothermal treatment the *β*-TCP was disappeared and the Hap was formed.

The morphology of Hap/PAN composite fiber mats were characterized by SEM (**Figure 2B, 2D),** and the structure resembles the brush-like morphology with Hap nanofibers as the bristles and PAN fiber as the backbone. **Figure 2B** showed the SEM images of Hap/PAN composite fiber mats with different vapor hydrothermal times at 140 ^{o}C. From **Figure 2B-5h** we can see that there were few Hap fibers growing out from the backbone PAN fiber, corresponding to the weak intensity of Hap peaks **(Figure 2A-5h)**. With the hydrothermal times increasing from 5 h to 24 h, the length of Hap fiber became larger. When the hydrothermal time reached 15 h and 24 h, the Hap turned out to be nanowire and uniformly distributed around the PAN fiber. **Figure 2D** presented the effect of hydrothermal temperature on the morphologies of Hap/PAN composite fibers. The Hap fiber became longer and more exuberant with the temperature increasing from 120 ^{o}C to 140 ^{o}C. When the temperature was up to 160 ^{o}C, the polymer PAN in the composite fiber mats was carbonized

because of the high temperature and pressure, although the morphology of Hap fibers was similar to that in Figure 4c. As was showin in **Figure 2C-160 °C**, the peak intensity of polymer was much weak than any other ones.

According to the above SEM and XRD results, the biomimetic growth process of Hap/PAN composite fiber mats can be described schematically as followed in **Figure 3**, TCP worked as the seed and it transferred to Hap nanofiber in situ and pierce the PAN fiber when it was cultured under high temperature vapor. With increasing of hydrothermal time, the length of Hap fiber became longer and PAN fiber could be densely coated by Hap nanowires after the process.

3.3 The structural analysis of Hap/PAN composite fiber

Through exploring the effect of hydrothermal temperature and time on the growth morphology of Hap/PAN composite fiber mats, we finally selected 140 °C and 15 h as the optimal hydrothermal condition to synthesize Hap/PAN composite fiber mats. The morphology and the size of the PAN/Hap composite fibers by 140 °C vapor hydrothermal trearment for 15 h were characteried by the SEM in **Figure 2D-140 °C** and TEM in **Figure 4**. The **Figure 2D-140 °C** provides a overview of the sample under different magnifications. The composite was composed by the backbone and the lateral brunches. The component of laterial brunch was Hap nanonwire which was converted by *β*-TCP and grow out from PAN fiber, as was confirmed by XRD pattern in **Figure 2C-15h.** To obtain the TEM images of the Hap nanowire in oder to Figure out the process of the Hap growth, DMF was adopted to disolve the PAN component of the PAN/Hap composite fiber mat. As shown in **Figure 4(A,B)**, the diamater of the Hap nanofiber was about 30 – 40 nm. The EDX spectrum of the Hap (**Figure 4E**) demonstrated that O, P and Ca elements were ascribed to Hap nanowire. The peak of

carbon and copper counld be attributed to the surface contamination and copper foil, respectively. The atomic ratio of Ca to P was about 1.5, which was close to the stoichiometry of calcium deficiency hydroxyapatite ($Ca_9(HPO_4)(PO_4)_5OH$). The crystalline structure of the HAP nanocrystals was further confirmed by the high-resolution TEM (HRTEM) investigations.**Figure 4C**, which was a microgram selected from **Figure 4B**, exhibited that the HAP crystal had the interplanar spacing of 0.348 nm, which corresponded to the (002) plane of hexagonal HAP. According to the SAED patter of the Hap (**Figure 4D**), the corresponding [-110] crystal axis can be indexed with reference to the hexagonal P63/m space group, using the Hap phase unit cell parameters. From the orientation relation between image of HRTEM and X-Ray diffraction, we can conclude that Hap followed c-axis growth, which agreed with the result of the relative stronger intensity of the (002) diffraction peak of PAN/Hap composite fiber.

General review of our previous works will be helpful to make clear why Hap in this work could be grown to nanowire. Rod-sHaped Hap (**Figure 5A**) were obtained by k. Ioko[15] who exposed the TCP sheet to the vapor of the pure water at the temperatures from 105 to 200 ◦C under the saturated vapor pressure for 1 - 20 h. **Figure 5B** showed the Hap granule prepared by Shidong ji[16], and spherical shape skeleton was replaced by rod-shaped Hap for α-TCP particles. Compared with Hap rods with the diameter of 2 - 3 μm synthesised (**Figure 5A, 5B**) in our previous works with vapor hydrothermal from TCP, the diameter of obtained-Hap fiber in this experience was about 30 - 40 nm (**Figure 5C**) which was much smaller. The reason causing the morphology differences of Hap is the diversity of mass transfer process in the process of vapor hydrothermal. A thick layer of water will be formed on the hydrophilous surface of TCP sheet and the TCP granule in the vapor

hydrothermal process, which will promote the reaction between TCP and H_2O. In our experience, due to the existence of hydrophobic PAN, there is only a thinner layer of water or discontinuous water droplets on the surface of TCP/PAN composite fiber. In adddtion to that, in the process of dissolution - recrystallization, the polymer matrix also impedes the combination of TCP. Considering that the mass transfer process is blocked, the much thinner Hap fibers will be formed and possess the ultrahigh-aspect-ratio at last.

3.4 Adsorption experiment results analysis:

From the SEM images of the Pb (II)-adorbed PAN/Hap composite fiber (the initail Pb^{2+} concentration was 250 ppm) in **Figure 6B**, we were surprised to find that a new substance was formed. **Figure 6A** was the XRD pattern of the Pb (II)- adorbed PAN/Hap composite fiber, through which we can see that the main phase is the pyromorphite ($Pb_{10}(PO_4)_6(OH)_2$, PbHA) and there are also week diffraction peaks of Hap existed. SEM results in **Figure 6B** did reveal morphological differences with respect to the initial Hap/PAN composite fiber (**Figure 2D-140◦C**). The morphologies of newly formed phase of pyromorphite have some discrepancies - in addition to the hexagonal flake appearance formation with the diamater of 3-4μm, there are also some rod-like pyromorphite appeared.

The value of pH variation dates in function of time was plotted in **Figure 7A** (the initail Pb^{2+} concentration was 250 ppm). The pH decreases from 5.2 to 3.7 at the first 20min stage, then the pH decreases slowly until the value of pH is located at 3.5. This result is correspond with the curve of figure 7C-250ppm.

What's more, there's an obvious phenomenon in the process of adsorption experience, which is the solution became a little turbid. Combined with the SEM picture and XRD pattern of the Pb (II)-adsorbed PAN/Hap composite fiber (**Figure 6**), we can reach the conclusion that the turbid component was PbHA and the dissolution of the hydroxyapatite followed by the reprecipitation of the pyromorphite was one of the important adsorption mechanisms, which can be described by the equations as follows:

$$Ca_{10}(HPO_4)(PO_4)_5(OH) \leftrightarrow 10Ca^{2+} + 5PO_4^{3-} + HPO_4^{2-} + OH^- \quad (3)$$

$$5PO_4^{3-} + HPO_4^{2-} + OH^- + H_2O + 10Pb^{2+} \leftrightarrow Pb_{10}(PO_4)_6(OH)_2 + 2H^+ \quad (4)$$

Figure 7B revealed the behavior of molar ratio ($Pb_{adsorbed}$ / $Ca_{solution}$) during the Pb^{2+} adsorption progress, from which we can see that the value decreased at the beginning of the reaction and at last the value was close to 0.8. These results suggestted that part of Pb^{2+} could be consumed by other mechanisms in addition to the dissolution - reprecipitation mechanism. One possibility is the metal complexation at the Hap surface as suggested by Xu and Schwartz[18] and Mavropoulos[19] who suggested that the metal ions, such as Cd^{2+} and Pb^{2+} are complexed at phosphate or Ca^{2+} sites displacing partially the H^+ ions. In the case of Pb^{2+}, this surface complexation can be written as follows:

$$\equiv POH + Pb^{2+} = \equiv POPb^+ + H^+ \quad (5)$$

$$\equiv PO^- + Pb^{2+} = \equiv POPb^+ + H^+ \quad (6)$$

$$\equiv CaOH + Pb^{2+} = \equiv CaOPb^+ + H^+ \quad (7)$$

Wu et al. studying the acid-base properties of apatite-water interface showed that when the solution pH < 6.0, 7.5<pH<9.0, and pH>10.5, the ≡POH, ≡PO^- and ≡CaOH are the predominant surface complex[18, 20], respectively. In this work, our initial pH value (<6) suggests that **Eq. (5)** should dominate in the first stage of the lead uptake: the proton leaching from ≡POH sites of Hap because of surface complexation of Pb^{2+} to form ≡$POPb^+$. The equations of dissolution - reprecipitation mechanism (**Eq. (3)(4)**) and the surface complexation mechanism (**Eq. (5)**) explained the reason why the value of pH decreased abruptly in the first short time.

3.4.1 The study of the absorption reaction kinetics.

The amount of adsorption (q_t) as a function of contact time was presented in **Figure 7C**. There is no comparable change in the concentration of Pb^{2+} ions with the contact time for the **Figure 7C-line 0**, so the influence of Pb^{2+} adsorption by PAN fiber can be excluded. The adsorption kinetics data were analyzed according to the pseudo-second-order kinetics:

$$t/q_t = 1/\left(k_2 q_e^{\ 2}\right) + t/q_e \qquad (7)$$

Where q_e and q_t are the amount of metal ions adsorbed (mg/g) at equilibrium and at time t, respectively; k_2 is the pseudo-second-order rate constant of adsorption (g/mg/min); and t is adsorption time (min).

Linear plot of t/q_t versus time t was shown in **Figure 7D**. The kinetic process for the adsorption of Pb^{2+} ions by PAN/Hap composite fiber mats perfectly followed the characteristics of the pseudo-second-order reaction model (R^2 = 0.99). From the intercept and slope linear plot of t/q_t vs. t, we can obtain the value of k_2 and q_e, which were 1.96 $\times 10^{-3}$, 3.38$\times 10^{-4}$, 8.13$\times 10^{-5}$, 1.38$\times 10^{-5}$ and

99.9, 198.5, 284.9, 427.35 for composite mats with the initial Pb^{2+} concentration of 125, 250, 375 and 500 mg/l, respectively.

3.4.2 Effect of initial Pb^{2+} concentration and the adsorption isotherm

The effect on different initial Pb^{2+} concentrations of 125, 250, 375 and 500 mg/l on the performance of the Hap/PAN composite fiber mat was investigated, and the initial pH value was controlled to be 5.2. **Figure 7C** is the adsorption amount of the Pb^{2+} with the different initial Pb^{2+} concentrations, from which we can see that the eventual amount of Pb^{2+} (q_e) adsorbed by the Hap/PAN composite fiber mat was risen from 100 mg/g to 427 mg/g with increasing the initial Pb^{2+} concentration.

Several isotherm models have been developed to illuminate the relationship between the extent of adsorption and the residual solute concentration, and the most widely used isotherm model is the Langmuir adsorption isotherm model, which is expressed as followed:

$$C_e/q_e = 1/(K_e \times q_{max}) + C_e/q_{max} \quad (8)$$

Where q_{max} (mg/g) is the maximum adsorption capacity; C_e (mg/l) is the Pb^{2+} equilibrium concentration in the solution; and K_e(l/g) is the Langmuir equilibrium constant, which is related to the binding energy of the metal ions to the active sites. The Langmuir isotherm of PAN/HAP composite mat for Pb^{2+} ions was shown in **Figure 7E**. The linear plot of C_e/q_e against C_e gives a good agreement with the Langmuir isotherm model (the correlation coefficient, R^2 = 0.9997). From the slope and the intercept, the value of q_{max} (433 mg/g) and C_e (0.696 l/g) can be acquired. Compared with other adsorbent materials listed in Table 1, the HAP/PAN composite mats prepared in this work exhibited an excellent adsorption capacity for metal Pb^{2+} ions.

Table 1:Adsorption capacities of Pb^{2+} ions by various adsorbents

adsorbent	q_{max}(mg/g)	reference
HAP/PAN	433	This work
Hydroxyapatite (70 wt.%)/polyacrylamide composite	209	[21]
Poorly crystalline hydroxyapatites synthesized from gypsum waste	500	[22]
Sodium tetraborate-modified kaolinite clay	42.92	[23]
Quebracho tannin resin	86.2	[24]
Calcium hydroxyapatite	85	[25]
HAP(50wt.%)/PAAm gel	178	[2]
HAP (50 wt.%)/PU composite foam	150	[4]

4. Conclusions

In summary, brush-like structure PAN/Hap composite fibers were successfully prepared by biomimetic process, combination of two simple but effective methods - electrospinning technology and vapor hydrothermal treatment. Owing to the large specific surface area of Hap, the maximum adsorption capacity of the composite fiber for Pb^{2+} reached 433mg/g. The removal of Pb^{2+}ions by

Hap can be explained by a two-step mechanism. Firstly, a rapid surface complexation of Pb^{2+} on the ≡POH sites of Hap nanowires was rapidly formed; then the dissolution of Hap in the composite fiber and precipitation of PbHA was dominant in the latter stage. The adsorption process obeyed the pseudo-second-order kinetics model very well. Excellent adsorption capacity for toxic metal ions and convenient access to recycling and reusing makes the biomimetic composite fiber mat a promising adsorbent for heavy metal ions from industrial waste water.

Notes and references

1. A. Corami, S. Mignardi and V. Ferrini, *J Colloid Interface Sci*, 2008, **317**, 402-408.
2. S. H. Jang, Y. G. Jeong, B. G. Min, W. S. Lyoo and S. C. Lee, *J Hazard Mater*, 2008, **159**, 294-299.
3. D. Liao, W. Zheng, X. Li, Q. Yang, X. Yue, L. Guo and G. Zeng, *J Hazard Mater*, 2010, **177**, 126-130.
4. S. H. Jang, B. G. Min, Y. G. Jeong, W. S. Lyoo and S. C. Lee, *J Hazard Mater*, 2008, **152**, 1285-1292.
5. L. Dong, Z. Zhu, Y. Qiu and J. Zhao, *Chem. Eng. J.*, 2010, **165**, 827-834.
6. R. Gonzalez-McQuire, J. Y. Chane-Ching, E. Vignaud, A. Lebugle and S. Mann, *J. Mater. Chem.*, 2004, **14**, 2277-2281.
7. J. D. Chen, Y. J. Wang, K. Wei, S. H. Zhang and X. T. Shi, *Biomaterials*, 2007, **28**, 2275-2280.
8. Y. X. Sun, G. S. Guo, D. L. Tao and Z. H. Wang, *Journal of Physics and Chemistry of Solids*, 2007, **68**, 373-377.
9. K. Lin, X. Liu, J. Chang and Y. Zhu, *Nanoscale*, 2011, **3**, 3052-3055.
10. C. M. Zhang, J. Yang, Z. W. Quan, P. P. Yang, C. X. Li, Z. Y. Hou and J. Lin, *Cryst. Growth Des.*, 2009, **9**, 2725-2733.
11. Y. W. Minhua Cao, Caixin Guo, and Y. Qi, 2004, 4784-4786.
12. Y. Z. Zhang, J. R. Venugopal, A. El-Turki, S. Ramakrishna, B. Su and C. T. Lim, *Biomaterials*, 2008, **29**, 4314-4322.
13. H. Wang, H. Tang, J. He and Q. Wang, *Mater. Res. Bull.*, 2009, **44**, 1676-1680.
14. P. A. Mouthuy, A. Crossley and H. Ye, *Materials Letters*, 2013, **106**, 145-150.
15. K. Ioku, G. Kawachi, S. Sasaki, H. Fujimori and S. Goto, *J. Mater. Sci.*, 2006, **41**, 1341-1344.
16. S. D. Ji, S. Murakami, M. Kamitakahara and K. Ioku, *Mater. Res. Bull.*, 2009, **44**, 768-774.
17. K. Ioku and S.Nishimura, *rev. high pressure sci. technol*, 1998, **7**, 1398-1400.
18. Y. P. Xu and F. W. Schwartz, *Journal of Contaminant Hydrology*, 1994, **15**, 187-206.
19. E. Mavropoulos, A. M. Rossi, A. M. Costa, C. A. C. Perez, J. C. Moreira and M. Saldanha, *Environmental Science & Technology*, 2002, **36**, 1625-1629.
20. Q. Y. Ma, S. J. Traina, T. J. Logan and J. A. Ryan, *Environmental Science & Technology*, 1993, **27**, 1803-1810.
21. S. H. Jang, B. G. Min, Y. G. Jeong, W. S. Lyoo and S. C. Lee, *J. Hazard. Mater.*, 2008, **152**, 1285-1292.
22. W. Yantasee, C. L. Warner, T. Sangvanich, R. S. Addleman, T. G. Carter, R. J. Wiacek, G. E. Fryxell, C. Timchalk and M. G. Warner, *Environmental Science & Technology*, 2007, **41**, 5114-5119.
23. S. Wang, T. Terdkiatburana and M. O. Tade, *Separation and Purification Technology*, 2008, **62**, 64-70.
24. M. Yurtsever and I. A. Sengil, *J. Hazard. Mater.*, 2009, **163**, 58-64.
25. A. Yasukawa, T. Yokoyama, K. Kandori and T. Ishikawa, *Colloid Surf. A-Physicochem. Eng. Asp.*, 2007, **299**, 203-208.

Associated content

Corresponding Author

Prof. Shidong Ji

Tel.: +86 21 69906206. Fax: +86 21 69906221. E-mail: sdki@mail.sic.ac.cn

Notes

The authors declare no competing financial interest.

Acknowledgements

This study was financially supported by the high-tech project of MOST (2014AA032802), the national sci-tech support plan the National Natural Science Foundation of China (NSFC, No.: 51372264), and the Science and Technology Commission of Shanghai Municipality (STCSM, No.: 13NM1402200).

Figures

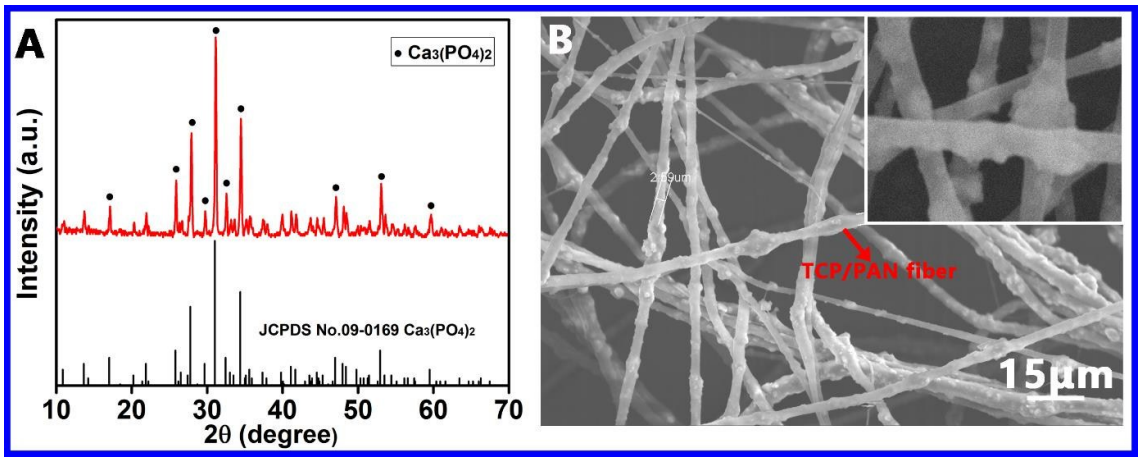

Figure 1. (A) XRD pattern of the product *β*-TCP synthesized at 1150 °C for 5 min; **(B)** SEM images of the PAN/TCP composite fiber and the inset is high magnifications. The diameter of the TCP/PAN composite fiber is 2-3μm.

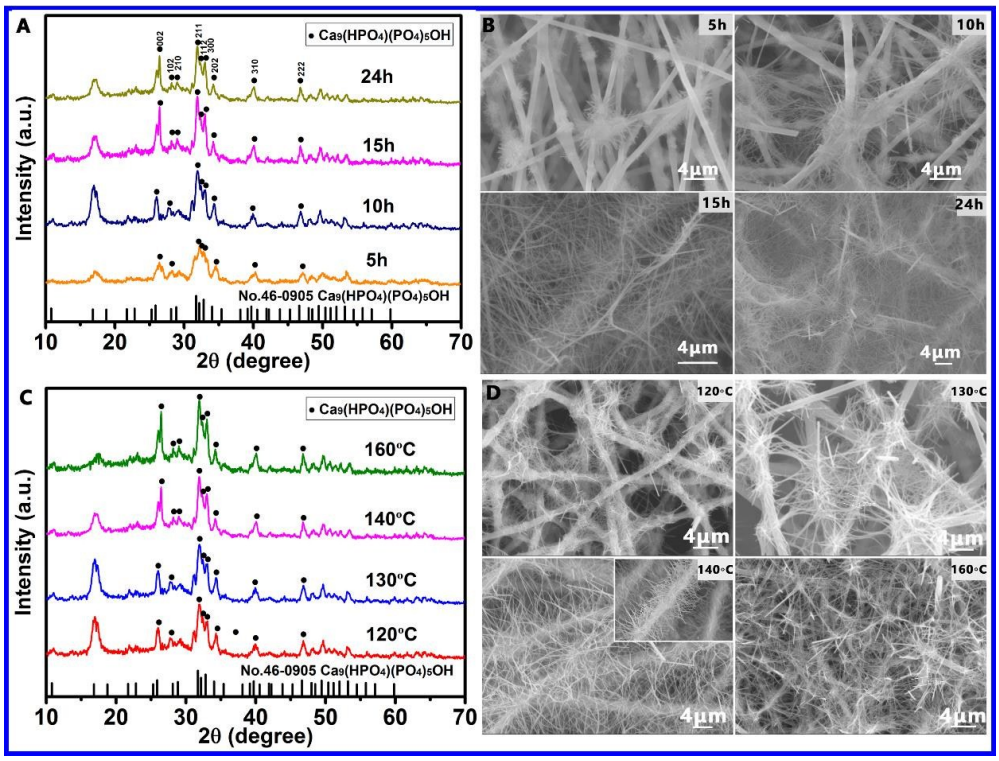

Figure 2. Preparation of Hap/PAN composite fiber mats in vapor hydrothermal condition. **(A)** XRD patterns of Hap/PAN composite fiber mats with different vapor hydrothermal times (5 h, 10 h, 15 h, 24 h) at 140 °C; **(B)** SEM images of Hap/PAN composite fiber mats with different vapor hydrothermal times (5 h, 10 h, 15 h, 24 h) at 140 °C. With the hydrothermal time increasing, the length of Hap is larger, and the Hap turned out to be nanowire and uniformly distributed around the PAN fiber. **(C)** XRD patterns of Hap/PAN composite fiber mats obtained by different vapor hydrothermal temperatures (120 °C, 130 °C, 140 °C, 160 °C) for 15 h; **(D)** SEM images of Hap/PAN composite fiber mats obtained for 15 h by different vapor hydrothermal temperatures (120 °C, 130 °C, 140 °C, 160 °C) for 15 h. The Hap fiber became longer and more exuberant at 140 °C, but at 160 °C, the PAN was carbonized, leading to the mats be fragmented.

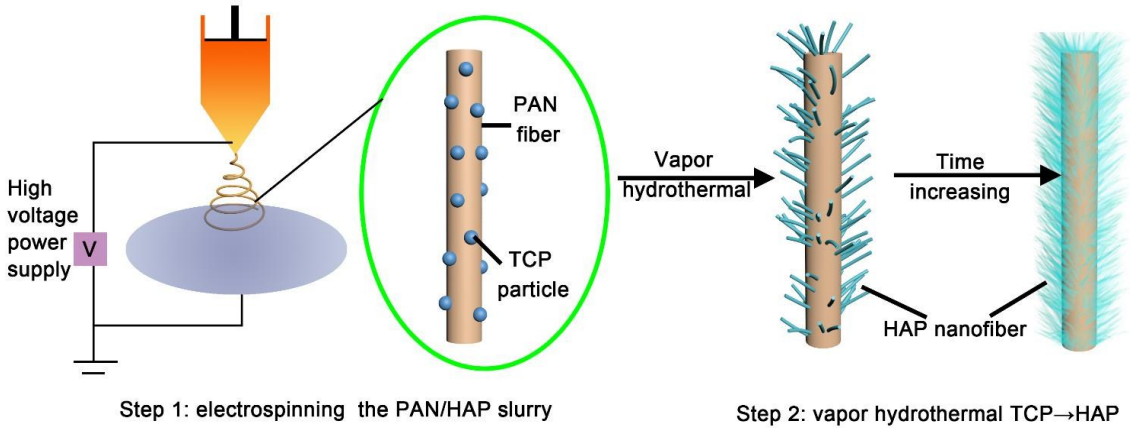

Figure 3. Biomimetic growth process diagram of Hap nanowires from PAN fibers

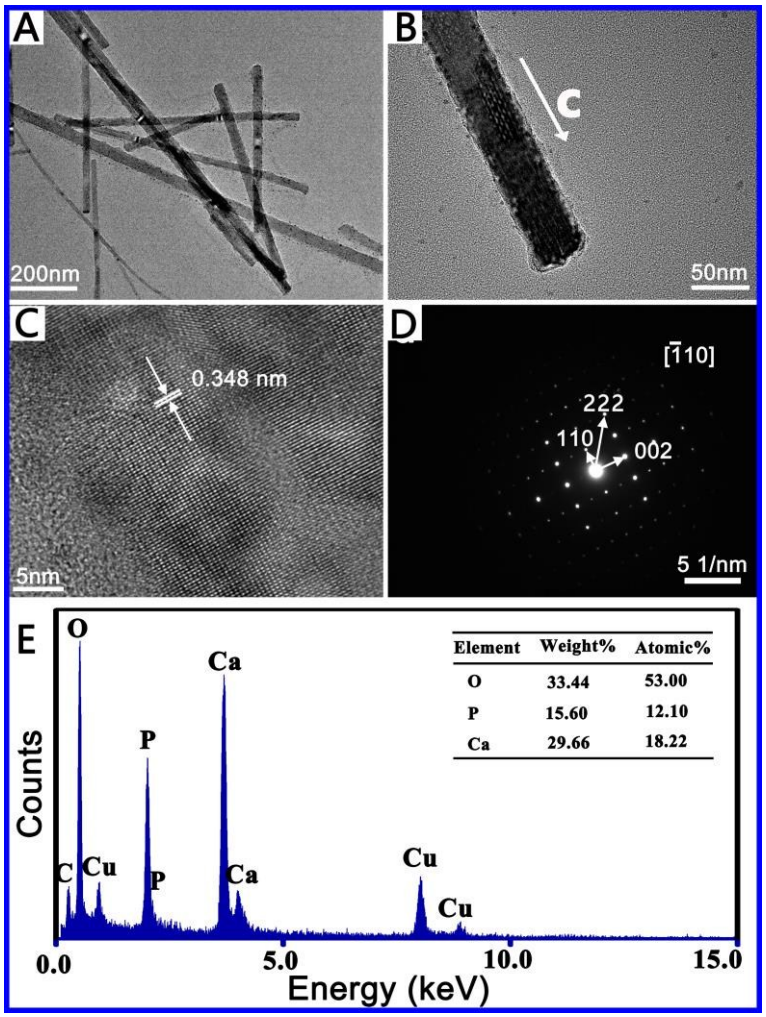

Figure 4. Characterization of Hap synthesised in our experience with the vapor hydrothermal at 140 °C for 15 h. **(A, B)** TEM images. The diameter of the Hap nanowire was 30 - 40nm. **(C)** HRTEM image. The interplanar spacing of 0.348 nm corresponds to the (002) lattice spacing. **(D)** SAED pattern; **(E)** EDX spectra. The atomic ratio of Ca to P in Hap was about 1.5, which was close to the stoichiometry of calcium deficiency hydroxyapatite($Ca_9(HPO_4)(PO_4)_5OH$).

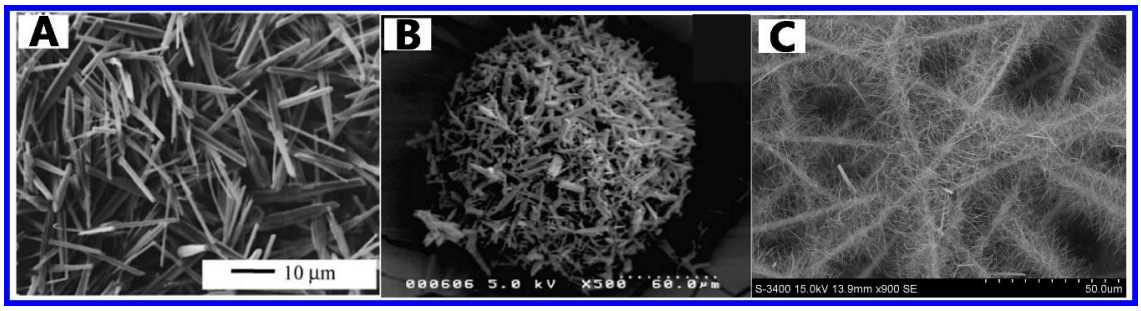

Figure 5. (A) Rod-sHaped Hap were obtained by k. Ioko who exposed the TCP sheet to the vapor of the pure water at the temperatures from 105 to 200°C under the saturated vapor pressure for 1 -20 h; **(B)** Hap granule prepared by Shidong ji, and spherical sHape skeleton was replaced by rod-sHaped Hap for α-TCP particles; **(C)** Hap/PAN composite fiber mat synthesised in our experience with the vapor hydrothermal at 140 °C for 15 h.

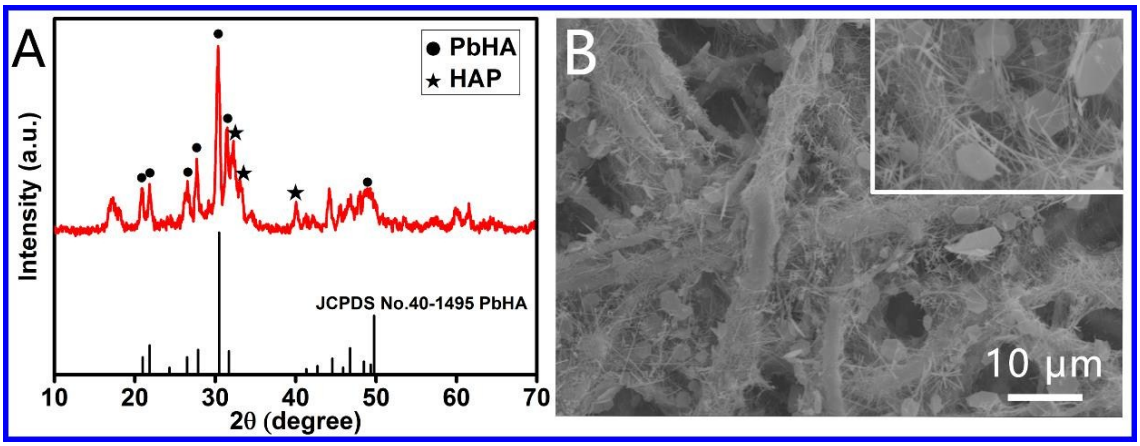

Figure 6. XRD pattern **(A)** and SEM images **(B)** of Pb(II)-adsorption PAN/Hap composite fiber (the initial Pb^{2+} concentration was 250 ppm).

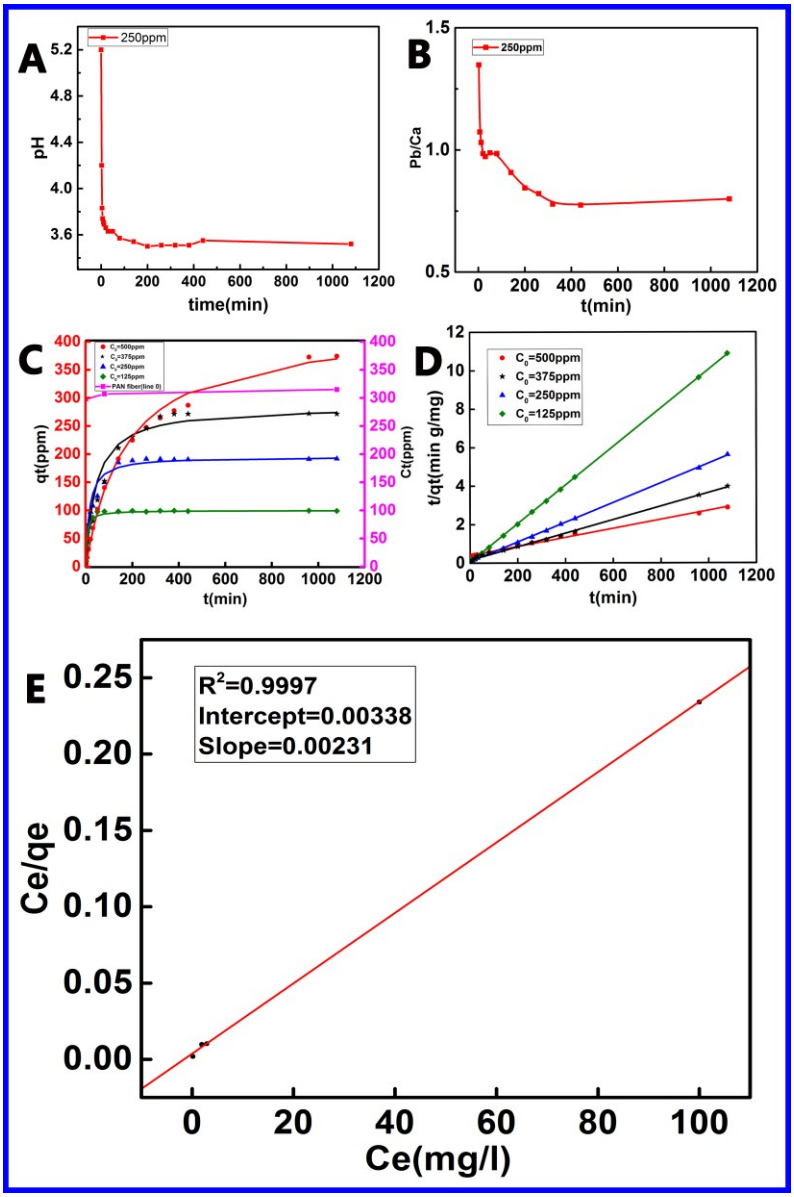

Figure 7. (A) The time-dependent pH value with the 250 ppm initial Pb^{2+} concentration; **(B)** the $Ca_{solution}/Pb_{adsorbed}$ molar ratio during the Pb^{2+} uptake with the 250 ppm initial Pb^{2+} concentration. **(C)** the time-dependent amount (q_t) of Pb^{2+} ions removed by Hap/HAP composite fiber mats (0.2 g) with various initail Pb^{2+} concentrations of 125 - 500ppm; **(D)** the removal kinetics analysis of Pb^{2+} ions with various initail Pb^{2+} concentrations of 125 – 500 ppm; **(E)** Langmuir isotherm plot for the adsorption of Pb^{2+} ions by PAN/HAP composite mats at pH 5.2.

A novel and functional ‘brush-like’ Hap/PAN composite was synthesized by a two-step method for the first time.

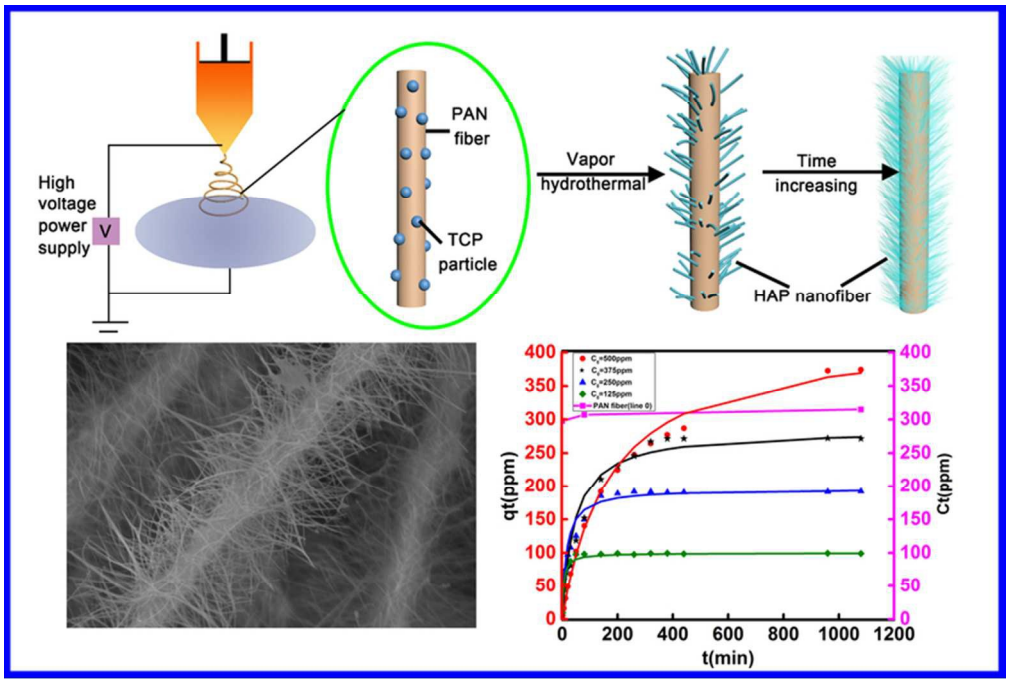

69x47mm (300 x 300 DPI)